Do Baby Brain Cortices that Look Alike at Birth Grow Alike During the First Year of Postnatal Development?

Rekik, Islem; Li, Gang; Lin, Weili; Shen, Dinggang

Published in:
Medical Image Computing and Computer Assisted Intervention – MICCAI 2018 - 21st International Conference, 2018, Proceedings

DOI:
10.1007/978-3-030-00931-1_65

Publication date:
2018

Document Version
Peer reviewed version

Do Baby Brain Cortices that Look Alike at Birth Grow Alike During The First Year of Postnatal Development?

Islem Rekik[1⋆], Gang Li[2], Weili Lin[2], and Dinggang Shen[2]

[1] BASIRA lab, CVIP group, School of Science and Engineering, Computing, University of Dundee, UK
[2] Department of Radiology and BRIC, University of North Carolina at Chapel Hill, NC, USA

Abstract. The neonatal brain cortex is marked with complex and high-convoluted morphology, that undergoes dramatic changes over the first year of postnatal development. A large body of existing research works investigating 'the developing brain' have focused on looking at changes in cortical morphology and charting the developmental trajectories of the cortex. However, the *relationship* between neonatal *cortical morphology* and its *postnatal growth trajectory* was poorly investigated. Notably, understanding the *multi-scale shape-growth relationship* may help identify early neurodevelopmental disorders that affect it. Here, we unprecedentedly explore the question: "Do cortices that look alike in shape at birth have similar kinetic growth patterns?". To this aim, we propose to analyze shape-growth relationship at three different scales. On a *global scale*, we found that neonatal cortices similar in geometric closeness are significantly correlated with their postnatal overall growth dynamics from birth till 1-year-old ($r = 0.27$). This finding was replicated when using shape similarity in morphology ($r = 0.20$). On a *local scale*, for both hemispheres, 20% of cortical regions displayed a significant high correlation ($r > 0.4$) between their similarities in morphology and dynamics. On a *connectional scale*, we identified hubs of cortical regions that were consistently similar in morphology and developed similarly across subjects including the cingulate cortex using a *novel integral shape-growth brain graph representation.*

1 Introduction

Little is known about how the cerebral cortex develops and works, particularly during early postnatal neurodevelopment [1]. Understanding the relationship between the neonatal cortical shape (i.e., geometry and morphology) and its postnatal kinetic behavior (i.e., dynamics[1] and velocity of growth) may produce novel diagnostic tools for better identifying neurodevelopmental disorders at a very early stage (e.g., schizophrenia and autism) [2, 3]. For instance, many brain disorders affect not only the cortex growth patterns, but also the cortex morphology [2]. However, the majority of existing studies investigate changes in cortical morphology or growth trajectories *independently*. To the best of our knowledge, the *multi-scale* relationship between the spatiotemporal

⋆ Corresponding author: islem.rekik@gmail.com, www.basira-lab.com
[1] Change in space and time or 4D change

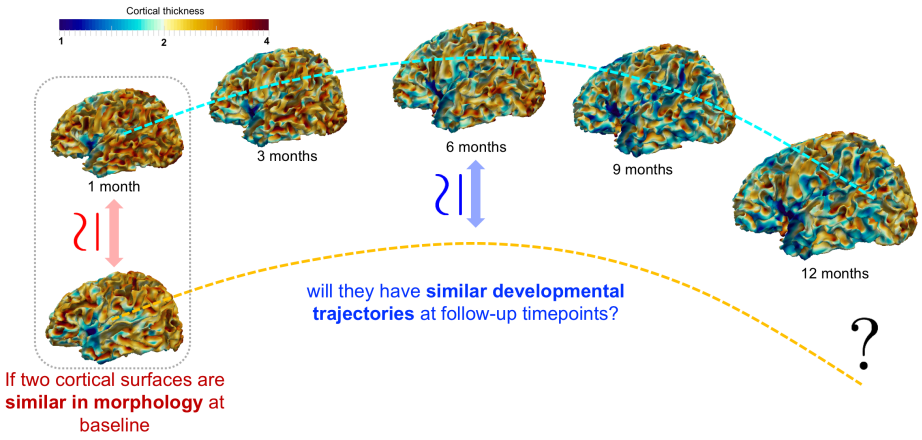

Fig. 1: *If two cortical shapes are similar in morphology at baseline (i.e., 1 month of age), will they have similar developmental trajectories at follow-up timepoints?*

dynamics and the morphology of the neonatal cerebral cortex is overlooked in the neuroscience literature.

To address this gap, we propose a multi-scale shape-growth analysis (MSGA) framework, which specifically investigates the following question: "Do cortices that look alike in shape at birth (both locally and globally) have similar kinetic growth patterns (e.g., velocity of growth) during the first year of postnatal development?" (**Fig. 1**). To this aim, we examine if *'similar'* shapes across individuals grow *'alike'* at three different scales: global, local and connectional. However, prior to developing our MSGA framework, one needs to define shape similarity and dynamic growth similarity metrics. Unlike several morphometric and volumetric analysis methods that cannot accurately characterize subtle cortical morphological changes in space and time, we leverage the multidirectional varifold-based cortical shape representation model introduced in [4] that quantifies the surface morphology along key directions at each vertex, and provides an informative metric that evaluates *morphological* similarity between shapes. We also use the Euclidean distance to evaluate the *geometric* closeness between shapes. As for the *kinetic*[3] *(or growth) similarity*, we use a longitudinal multidirectional varifold regression model based on [4], which allows to estimate the spatiotemporal velocity of each vertex in the baseline cortical surface within a specific time-window starting at first acquisition timepoint. Next, we propose a pairwise correlation-based similarity that quantifies the dynamic co-behavior in two different locations (or regions) of the neonatal cortex.

At a global scale, we examine the correlation between morphologically (resp. geometrically) similar neonatal cortical shapes and their kinetic developmental trajectories. At a local scale, we examine shape-velocity correlations in very distinctive cortical regions. Finally, at a connectional scale, inspired from [5], we further propose a novel integral brain 'shape-growth' graph representation to identify neonatal cortical regions

[3] Related to the velocity of shape deformation.

that are similar in morphology, but also grow similarly in respectively the left and the right hemispheres.

2 Multi-scale Shape-Growth Analysis (MSGA) Framework

To investigate if two similar shapes at baseline (first acquisition timepoint) will develop similarly over time, we introduce the key ingredients of our proposed MSGA framework as follows.

Quantification of cortical shape morphology using multi-directional varifold representation. First, we use the multidirectional varifold shape representation proposed in [4] to quantify the morphology of a cortical surface S at each mesh (triangular face) center x_i along two orthogonal directions: the non-oriented normal direction $\overleftrightarrow{n_i}$, and the non-oriented maximum principal curvature direction $\overleftrightarrow{\kappa_i}$. Specifically, a surface S with M meshes (triangles) is approximated by the sum of Dirac varifolds evaluated at the positions x_i of the centers of its M meshes using their corresponding non-oriented normals $\overleftrightarrow{n_i}$ and non-oriented maximum principal curvature direction $\overleftrightarrow{\kappa_i}$: $S = \sum_{i=1}^{M} \delta_{(x_i, \overleftrightarrow{n_i})} + \delta_{(x_i, \overleftrightarrow{\kappa_i})}$. More importantly, the varifold space W^* is endowed with a dot-product that enables to measure the morphological similarity between two shapes $S = \sum_i \delta_{(x_i, \overleftrightarrow{n_i})} + \delta_{(x_i, \overleftrightarrow{\kappa_i})}$ and $S' = \sum_j \delta_{(x'_j, \overleftrightarrow{n'_j})} + \delta_{(x'_j, \overleftrightarrow{\kappa'_j})}$ are: $< S, S' >_{W^*} = \sum_i \sum_j K_W(x_i, x'_j)(\frac{(n_i^T n'_j)^2}{|n_i||n'_j|} + \frac{(\kappa_i^T \kappa'_j)^2}{|\kappa_i||\kappa'_j|})$, where K_W is a Gaussian kernel that decays at rate σ_W. We note that σ_W represents the scale under which morphological details of the cortical shape are overlooked.

Quantification of cortical developmental trajectories using multi-directional varifold regression model. Given a set of shapes $\{S^1, \ldots, S^{N_S}\}$, we nest each of these into a multidirectional varifold space W^*, where each shape S^k (i.e., $k-$th subject in the population) is represented as a sum of two 'orthogonal' varifolds. Since each shape is measured longitudinally at different timepoints $t \in [0, 1]$, we estimate its evolution trajectory through deforming the baseline multidirectional varifold S_0^k onto a set of target multidirectional varifolds $\{S_1^k, \ldots, S_T^k\}$ respectively observed at different observation timepoints. To do so, we model this longitudinal shape deformation from baseline as a minimization problem [4]: $J_{W^*} = \frac{1}{2} \int_0^1 ||v_t||_V^2 dt + \gamma \sum_{j \in \{1,\ldots,T\}} ||S_{t_j}^k - \phi(S_0^k, t_j)||_{W^*}^2$, where γ represents a trade-off between the deformation smoothness energy and the similarity between ground-truth and deformed shapes. $\phi(\mathbf{x}, t),\ t \in [0, 1]$ represents a smooth invertible deformation (i.e., diffeomorphism), fully defined by a set of N_z control points z_i and their attached initial deformation momenta α_i. We fix the N_z control points across all subjects, to compare their growth trajectories. v_t denotes the estimated smooth shape deformation velocity field, which belongs to a reproducing kernel Hilbert space V, spanned by Gaussian kernel K_V with standard deviation σ_V. Specifically, the vertex-wise spatiotemporal piece-wise continuous velocity v is defined at a location $\mathbf{x}$ and timepoint t as: $v(\mathbf{x}, t) = \sum_{i=1}^{N_z} K_V(\mathbf{x}, z_i(t))\alpha_i(t)$. Notably, this multidirectional varifold deformation framework allows to establish vertex-to-vertex correspondence across subjects and timepoints. Next, we leverage the multidirectional varifold for shape representation and the estimated velocity for growth quantification to compute morphological similarity and growth similarity between pairs of shapes in our cohort.

Geometric shape similarity matrix definition. To quantify the *geometric* concordance between two neonatal surfaces S_i and S_j, we use the Euclidean distance as follows: $d(S_i, S_j) = \sum_{x=1}^{N} ||S_i(x) - S_j(x)||_2$, where N represents the number of vertices. We then transform the pairwise distance into a pairwise similarity using a continuous mapping ($f(x) = x^2 - 2x + 1$). Unlike non-smooth linear regression mapping, the proposed non-linear function f is continuously differentiable (or smooth), which helps better preserve the potential local smoothness that may exist in the original shape similarity matrix. Next, we generate an $N_s \times N_s$ matrix $\mathcal{S}_g$, where each element $\mathcal{S}_g(i, j)$ quantifies the similarity in geometry between two shapes S^i and S^j.

Morphological shape similarity matrix definition. In a similar way, we generate a morphological shape dissimilarity matrix, where each element measures the dissimilarity in morphology between two shapes S^i and S^j using the multidirectional varifold distance norm $||S_i - S_j||_{W^*}$. We also reverse this matrix using the f-mapping to finally get the morphological shape similarity matrix $\mathcal{S}_m$.

Velocity similarity matrix definition. To measure the similarity in developmental dynamics of two baseline shapes, we first retrieve at each vertex x_i in the baseline surface S^0 the estimated spatiotemporal velocity signal along first, second, and third axes: $\mathbf{v^1}(x_i) = [v^1(t = 0, x_i), \ldots, v^1(t = T, x_i)]$, $\mathbf{v^2}(x_i) = [v^2(t = 0, x_i), \ldots, v^2(t = T, x_i)]$, and $\mathbf{v^3}(x_i) = [v^3(t = 0, x_i), \ldots, v^3(t = T, x_i)]$. Then, we generate the coordinate-wise Pearson correlation with its corresponding vertex x_j in a different baseline surface S^j. Finally, we compute their average and store it in an element $\mathcal{G}_v(i, j)$ of the velocity $N_s \times N_s$ similarity matrix: $\sum_{x=1}^{N} \frac{1}{N}(corr^2(\mathbf{v^1}(x_i), \mathbf{v^1}(x_j)) + corr^2(\mathbf{v^2}(x_i), \mathbf{v^2}(x_j) + corr^2(\mathbf{v^3}(x_i), \mathbf{v^3}(x_j)))^{1/2}$.

Initial momenta similarity matrix definition. Here, for each pair of neonatal cortical shapes S^i and S^j in our cohort, we compute the average inner product between their respective initial deformation momenta, and then assign this value, which lies in the interval $[-1, 1]$, to an element (i, j) of an $N_s \times N_s$ matrix $\mathcal{G}_m$ that sparsely quantifies how similar is the 4D deformation of both shapes.

Global shape-growth analysis. At a global scale, we compute the Pearson correlation between only the halves of the geometric similarity shape matrix $\mathcal{S}_g$ and the initial momenta similarity matrix $\mathcal{G}_m$ as they are symmetric. We also compute the correlation between the morphological similarity shape matrix $\mathcal{S}_m$ and $\mathcal{G}_m$. To better examine the global dense deformation trajectories, we compute the correlation between both geometric $\mathcal{S}_g$ and morphological $\mathcal{S}_m$ matrices and the global velocity similarity matrix $\mathcal{G}_v$ computed on the whole cortex.

Local ROI-based shape-velocity co-behavior analysis. To investigate the variation in strength of the shape-growth correlates in different local cortical regions, we parcellate each cortical surface into N_r anatomical regions of interest (ROIs). Then, we generate *for each ROI* r a velocity similarity matrix $\mathcal{G}_v^r$ of size $N_s \times N_s$. **Supp. Fig. 1**[1] illustrates this step for a representative cortical region. On a local scale, to examine if baseline cortical regions that look similar have correlated postnatal dynamic behavior, we also create for each ROI a morphological shape similarity matrix $\mathcal{S}_m^r$ to assess the regional morphological similarity between individuals and geometric shape similarity matrix $\mathcal{S}_g^r$ to assess the regional geometric concordance or closeness. Then, for each

[1] Supplementary material link: http://basira-lab.com/wp-content/uploads/2017/05/Supp-Rekik-et-al.-MICCAI-2018.pdf

hemisphere and for each ROI, we compute the Pearson correlation coefficient between a velocity similarity matrix $\mathcal{G}_v^r$ and each shape similarity matrix ($\mathcal{S}_g$ and $\mathcal{S}_m$).

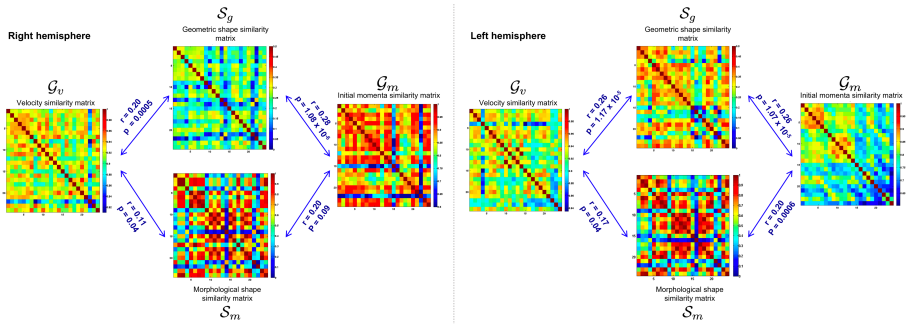

Fig. 2: *Global analysis: Correlation between shape similarity and velocity similarity matrices*. For each hemisphere, we computed the correlation between the geometric (vs. morphological) shape similarity matrix with respectively initial momenta similarity matrix and velocity similarity matrix.

Connectional shape-growth analysis. To identify regional cortical connections that show strong correlation between regions that look alike and grow alike *across all subjects*, we first define for each subject s shape $\mathcal{S}_m^s$ and growth $\mathcal{G}_v^s$ matrices, each of size $N_r \times N_r$. Next, we fuse all morphological shape matrices to generate the morphome (**Supp. Fig. 2**), and all velocity-based growth matrices to generate the kinectome using network fusion method proposed in [6]. Next, for each hemisphere, we normalize both fused shape connectivity and mean velocity connectivity matrices, then we compute their absolute difference matrix. Through sparsifying the matrix by retaining only the $P_s\%$ lowest difference values, we unprecedentedly define the *morpho-kinetome*, where similar cortical regions in morphology have correlated growth trajectories and dissimilar brain regions have uncorrelated growth trajectories. We illustrate in **Supp. Fig. 3** three cases where we generate morpho-kinectomes at different sparsification levels and with different scales in shape-growth co-behavior.

3 Results and Discussion

Data and parameter setting. In this study, we used 115 MR images from 23 healthy full-term born infants. Each infant was scheduled to be scanned at 5 time points (1, 3, 6, 9, and 12 months of age). At each scheduled scan, T1-, T2-, and diffusion-weighted MR images were acquired by a Siemens 3T head-only MR scanner with a 32 channel head coil. T1-weighted images (144 sagittal slices) were acquired with the imaging parameters: $TR = 1900ms$, $TE = 4.38ms$, flip angle $= 7$, acquisition matrix $= 256 \times 192$, and voxel size $= 1 \times 1 \times 1mm^3$. T2-weighted images (64 axial slices) were acquired with the imaging parameters: $TR/TE = 7380/119ms$, flip angle $= 150$, acquisition matrix $= 256 \times 128$, and voxel size $= 1.25 \times 1.25 \times 1.95mm^3$. We parcellated each cortical hemisphere into 35 ROIs using the Desikan-Killiany atlas. For the multidirectional varifold-based geodesic shape regression model, we empirically set $\gamma = 10^{-4}$, $\sigma_W = 5$, and $\sigma_V = 25$.

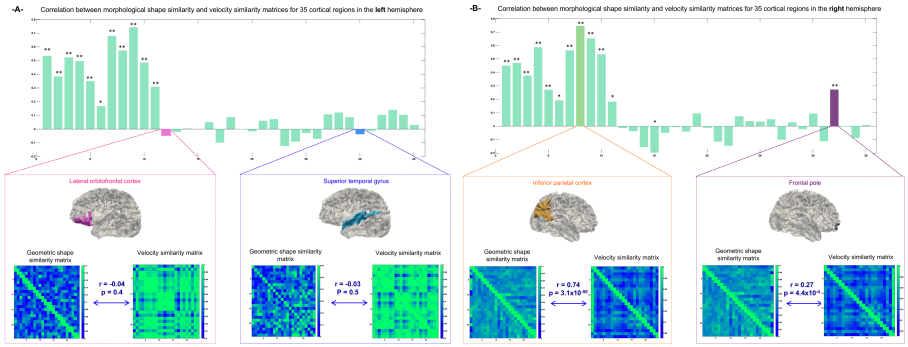

Fig. 3: *Local ROI-based shape-growth correlation analysis for left and right hemispheres in developing brains.* Correlation for each cortical region of interest between geometric shape similarity matrix and velocity similarity matrix. $**$ denotes highly significant correlations ($p \ll 10^{-3}$) and $*$ denotes significant correlation ($p < 0.05$).

Global shape-growth analysis. Our global analysis revealed a significantly positive correlation between geometrically close shapes and their growth dynamics as well as between similar shapes in morphology and their dynamic evolution. In particular, as shown in **Fig.** 2, the initial momenta similarity matrix correlated with the geometric shape similarity matrix in both left ($r = 0.26,\ p = 1.07 \times 10^{-5}$) and right ($r = 0.28,\ p = 0.09$) hemispheres, and slightly less correlated with the morphological shape similarity matrix ($r = 0.20,\ p < 10^{-5}$) in both hemispheres. This is quite expected since the varifold metric captures the richness and complexity of the cortical foldings that largely vary between subjects, unlike the geometric similarity that grossly approximates closeness between cortical surfaces. In addition, to not reduce the cortical growth to only a sparse set of initial momenta, we also use the velocity similarity matrix which encodes the mean correlation between all vertex-wise velocity trajectories in x, y and z spatial directions. Our findings also revealed a positive correlation between the velocity similarity matrix and the geometric shape similarity matrix in both left ($r = 0.26,\ p = 1.17 \times 10^{-5}$) and right ($r = 0.20,\ p = 5 \times 10^{-4}$) hemispheres, which similarly decreased when using the morphological shape similarity matrix for the left ($r = 0.17,\ p = 0.04$) and the right ($r = 0.11,\ p = 0.04$) hemispheres.

Local shape-growth analysis. We extended our previous findings by exploring the shape-velocity co-behavior in 35 cortical regions. For each ROI, we computed the Pearson correlation coefficient between the velocity similarity matrix and the morphological shape similarity matrix. For both left and right hemispheres, 20% of the cortical regions had a statistically significant high correlation between their morphological closeness and growth dynamics ($r > 0.4,\ p \ll 0.001$) (**Fig.** 3). These included for both hemispheres the superior temporal sulcus, caudal middle frontal gyrus, fusiform gyrus, inferior parietal cortex, inferior temporal gyrus and isthmus cingulate cortex, along with the right anterior cingulate cortex –mainly belonging to the temporal, frontal and limbic lobes. We also found statistically nonsignificant negative correlations in about 10 cortical regions using the morphological similarity. For the right hemisphere, 13/35 regions had negative correlations where only the middle temporal gyrus was statistically significant ($p < 0.05$). Clearly, both cortical hemispheric developments are marked by correlated and anti-correlated shape-velocity behaviors largely consistent across cor-

tical regions, where distinctive cortical areas exhibited highly significant correlation values. Our findings also suggest that *specific* cortical regions such as the inferior parietal cortex (IPC) in both left and right hemispheres, which is part of the default mode network and is involved in interpretation of sensory information, language and body image, exhibited a powerful positive correlation between their shape and growth similarity matrices ($r > 0.7$).

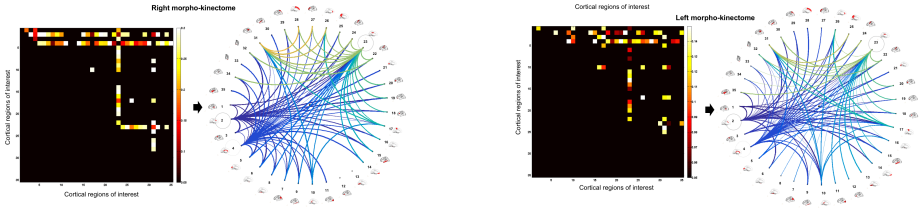

Fig. 4: *The morpho-kinectome.* Each node in the circular graph denotes a cortical region as in **Supp. Fig. 4**. Each color defines one node. The width of a circular edge represents its strength. The circular graph shows that both left and right morpho-kinectomes share two key cortical hubs: node 2 (the caudal anterior-cingulate cortex) and node 23 (posterior-cingulate cortex). We would like to note that node 4 representing the corpus callosum is overlooked as it is not part of the cortex.

Connectional shape-growth analysis using the proposed morpho-kinectome. In the right and left morpho-kinectomes sparsified at $P_s = 15\%$, we found that the caudal anterior-cingulate cortex (ACC) and posterior-cingulate cortex (PCC) presented the key hubs (**Fig. 4**). Noting that developmental studies suggest that structural hubs emerge relatively early during brain development, with connectivity of posterior cingulate regions already present in the postnatal brain [7], can potentially explain the shape-growth co-behavior of neonatal cingulate regions. The cingulate cortex is involved in spatial memory, configural learning, and maintenance of discriminative avoidance learning, which are fundamental cognitive functions to infants' development and learning [8, 7]. Importantly, relating the morpho-kinectome to growth connectomics and neurodevelopment [9] as well as genetic [10] and developmental [11] underpinnings would give insights into neurodevelopment and the etiology of neurodevelopmental disorders.

4 Conclusion

In sum, our MSGA framework demonstrated that globally similar cortical shapes similarly co-evolve. We also identified distinctive cortical regions (e.g., IPC) that grow similarly when looking similar in morphology –which may indicate that their growth is controlled by similar genetic and biological factors. We also showed that shape connectivity is a powerful predictor of growth dynamics in specific cortical regions (e.g., anterior/posterior cingulate cortices). The model presented here is a highly promising starting point, given that it can be generalized to different complex shapes and allows to examine the spatiotemporal dynamics of shapes as well as quantifying their high-dimensional (here 3D) morphology. Besides, it will be more intriguing to interpret our

findings in the light of multiple covariates such as stress during development [12] and socio-economic status of recruited infants, as both are suspected to affect early brain development [13]. Eventually, our proposed MSGA framework may help better elucidate how the cortex develops and wires itself in both healthy and disordered infant brains as well as provide a comprehensive graph-based brain representation that unifies genetics, connectomics and *morpho-kinectomics*.[1]

References

1. Li, G., Wang, L., Yap, P.T., Wang, F., Wu, Z., Meng, Y., Dong, P., Kim, J., Shi, F., Rekik, I., et al.: Computational neuroanatomy of baby brains: A review. NeuroImage (2018)
2. Dubois, J., Benders, M., Borradori-Tolsa, C., Cachia, A., Lazeyras, F., Leuchter, R.H.V., Sizonenko, S., Warfield, S., Mangin, J., Huppi, P.: Primary cortical folding in the human newborn: an early marker of later functional development. Brain **131** (2008) 2028–2041
3. Wallace, G., Dankner, N., Kenworthy, L., Giedd, J., Martin, A.: Age-related temporal and parietal cortical thinning in autism spectrum disorders. Brain **133** (2010) 3745–3754
4. Rekik, I., Li, G., Lin, W., Shen, D.: Multidirectional and topography-based dynamic-scale varifold representations with application to matching developing cortical surfaces. Neuroimage **135** (2016) 152–162
5. Rekik, I., Li, G., Lin, W., Shen, D.: Estimation of shape and growth brain network atlases for connectomic brain mapping in developing infants. Biomedical Imaging (ISBI 2018), 2018 IEEE 15th International Symposium on (2018) 985–989
6. Wang, B., Mezlini, A., Demir, F., Fiume, M., Tu, Z., Brudno, M., Haibe-Kains, B., Goldenberg, A.: Similarity network fusion for aggregating data types on a genomic scale. Nat Methods **11** (2014) 333–337
7. Heuvel, M.V.D., Sporns, O.: Network hubs in the human brain. Trends Cogn Sci **17** (2013) 683–696
8. Maddock, R., Garrett, A., Buonocore, M.: Remembering familiar people: the posterior cingulate cortex and autobiographical memory retrieval. Neuroscience **104** (2001) 667–676
9. Vertes, P., Bullmore, E.: Annual research review: Growth connectomics–the organization and reorganization of brain networks during normal and abnormal development. J Child Psychol Psychiatry **56** (2015) 299–320
10. Panizzon, M., Fennema-Notestine, C., Eyler, L., Jernigan, T., Prom-Wormley, E., Neale, M., Jacobson, K., Lyons, M., Grant, M., Franz, C., Xian, H., Tsuang, M., Fischl, B., Seidman, L., Dale, A., Kremen, W.: Distinct genetic influences on cortical surface area and cortical thickness. Cereb Cortex **19** (2009) 2728–2735
11. Raznahan, A., Shaw, P., Lalonde, F., Stockman, M., Wallace, G., Greenstein, D., Clasen, L., Gogtay, N., Giedd, J.: How does your cortex grow? J Neurosci **31** (2011) 7174–7177
12. Hanson, J., Chung, M., Avants, B., Rudolph, K., Shirtcliff, E., Gee, J., Davidson, R., Pollak, S.: Structural variations in prefrontal cortex mediate the relationship between early childhood stress and spatial working memory. J Neurosci **32** (2012) 7917–7925
13. Brito, N., Noble, K.: Socioeconomic status and structural brain development. Front Neurosci **8** (2014) 276

[1] This work was supported by NIH grants (MH100217, MH107815, MH108914, and MH110274).

Do Baby Brain Cortices that Look Alike at Birth Grow Alike During The First Year of Postnatal Development? (Supplementary Material)

Islem Rekik[1⋆], Gang Li[2], Weili Lin[2], and Dinggang Shen[2]

[1] BASIRA lab, CVIP group, School of Science and Engineering, Computing, University of Dundee, UK
[2] Department of Radiology and BRIC, University of North Carolina at Chapel Hill, NC, USA

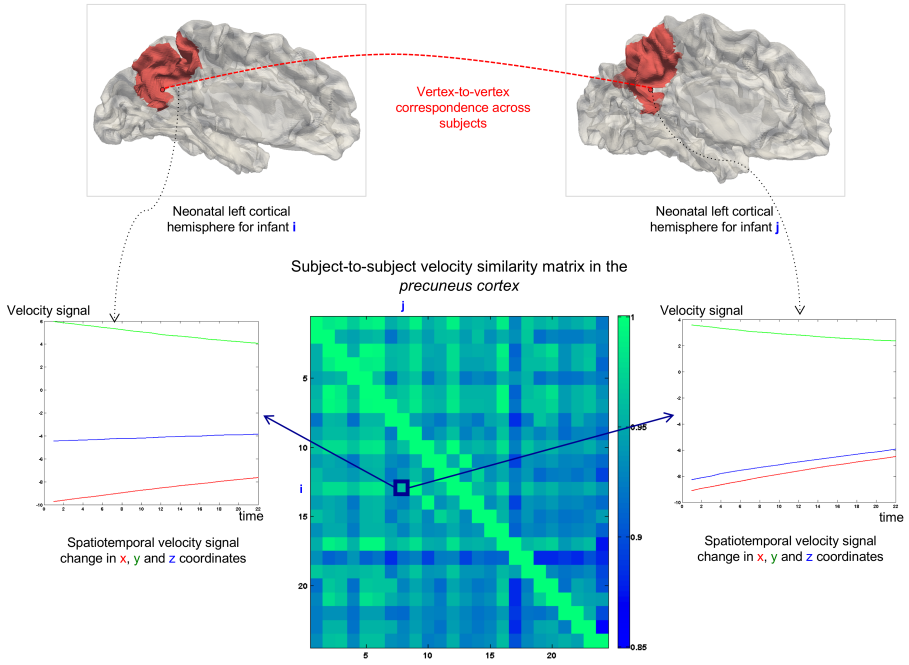

Fig. 1: *Subject-to-subject velocity similarity matrix in a representative cortical region (the precuneus).* The multidirectional varifold-based shape regression model enables to estimate for each subject the spatiotemporal deformation velocity $v(x,t)$ which is computed at each vertex x of the cortical surface and at any timepoint t between birth and 12 months. Then, for each cortical region, we generate a velocity similarity matrix that computes the Pearson correlation coefficients between corresponding vertices in two infants i and j averaged across the selected region.

⋆ Corresponding author: irekik@dundee.ac.uk, www.basira-lab.com

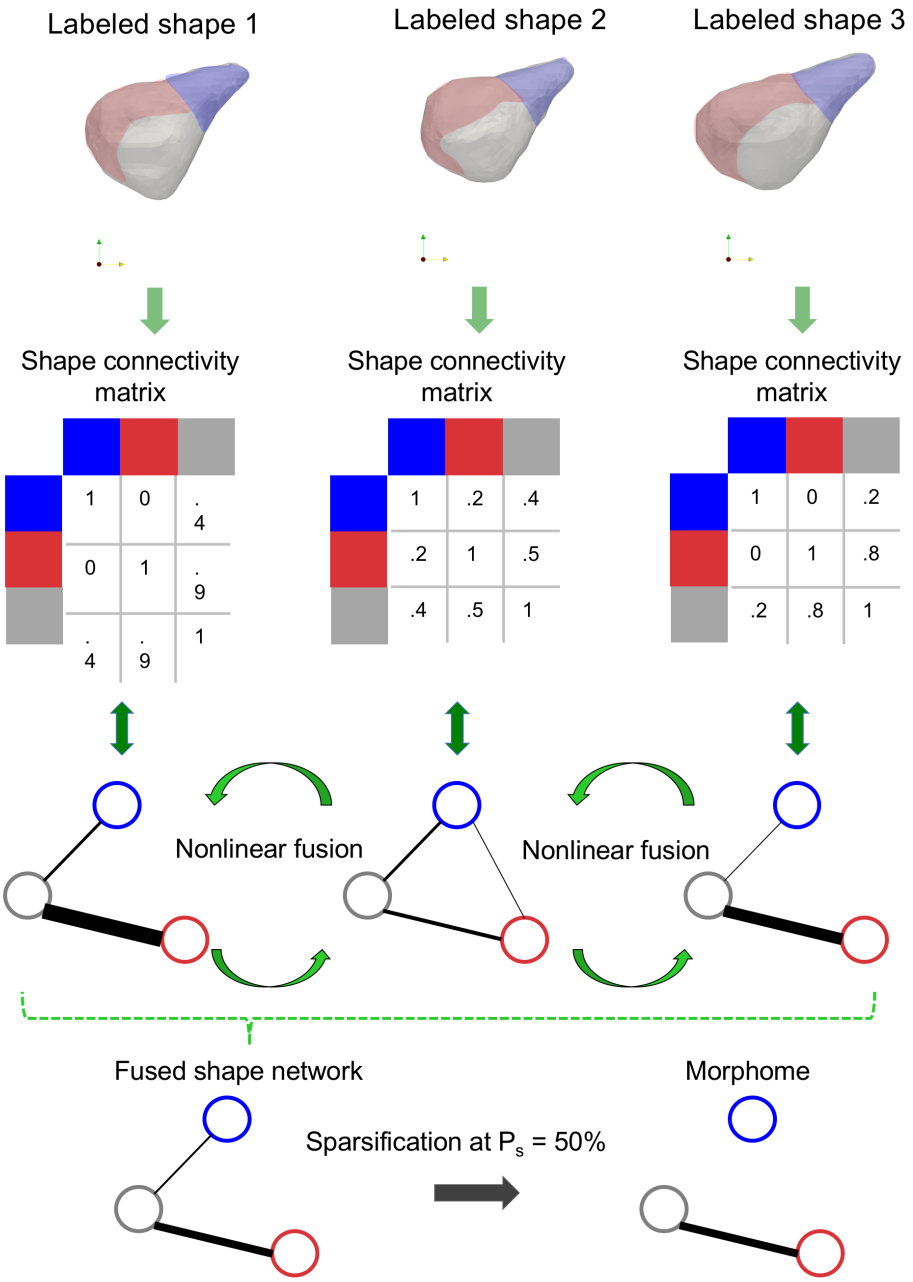

Fig. 2: *Generic shape similarity networks fusion and morphome construction.* Giving a set of labeled shapes measured at a single timepoint, we use the multi-directional varifold similarity distance to compute pairwise similarities between different labeled regions for each shape. This produces a shape connectivity matrix for each labeled shape. Next, we use the non linear similarity network fusion method described in [4] to generate the 'mean' shape network. Ultimately, through removing 50% of the remaining connections, we generate a morphome at a sparcification level $P_s = 50\%$.

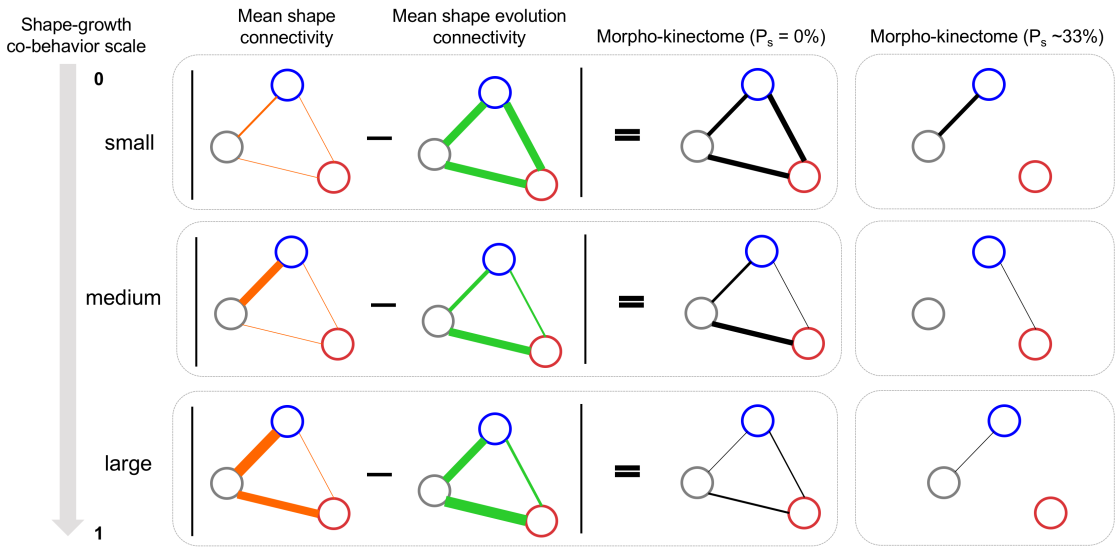

Fig. 3: *Morpho-kinectomes generation scenarios at different sparsification levels* P_s. To better explain the intuition behind introducing the concept of the morpho-kinectome in this paper, we illustrate three cases that represent different levels of shape-growth consistency in similarity patterns, each respectively drawn from an observed population of longitudinal shapes. Each node represents a labeled anatomical region in the observed shape. The width of each edge quantifies the similarity between two nodes in the network. The mean shape connectivity network is estimated at baseline timepoint whereas the mean shape evolution connectivity network is estimated across later acquisition timepoints. The shape-growth consistency level or co-behavior ranges between a scale of 0 and 1. As the shape-growth co-behavior scale increases, the fully connected weighted morpho-kinectome (i.e., $P_s = 0\%$) involves weaker connections between its nodes. Notably, the stronger the connections in the morpho-kinectome, the less coordinated are similar labeled shape regions in appearance and evolution. We also demonstrate how the sparsification level influences the sparsity of the estimated morpho-kinectome, which is defined as a weighted sparse network at $P_s > 0$.

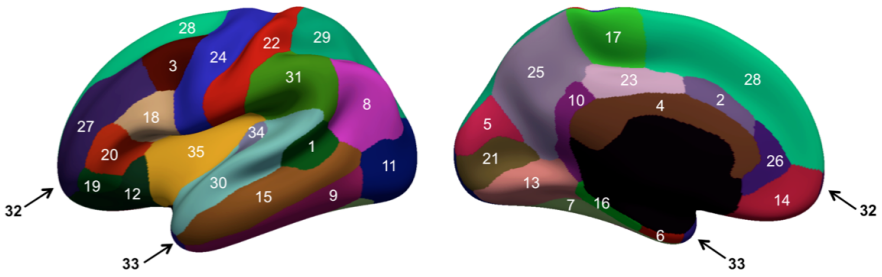

1. Bank of the Superior Temporal Sulcus	**2.** Caudal Anterior-cingulate Cortex
3. Caudal Middle Frontal Gyrus	**4.** Unmeasured Corpus Callosum
5. Cuneus Cortex	**6.** Entorhinal Cortex
7. Fusiform Gyrus	**8.** Inferior Parietal Cortex
9. Inferior Temporal Gyrus	**10.** Isthmus-cingulate Cortex
11. Lateral occipital cortex	**12.** Lateral orbital frontal cortex
13. Lingual gyrus	**14.** Medial orbital frontal cortex
15. Middle temporal gyrus	**16.** Parahippocampal gyrus
17. Paracentral lobule	**18.** Pars opercularis
19. Pars orbitalis	**20.** Pars triangularis
21. Pericalcarine cortex	**22.** Postcentral gyrus
23. Posterior-cingulate cortex	**24.** Precentral gyrus
25. Precuneus cortex	**26.** Rostral anterior cingulate cortex
27. Rostral middle frontal gyrus	**28.** Superior frontal gyrus
29. Superior parietal cortex	**30.** Superior temporal gyrus
31. Supramarginal gyrus	**32.** Frontal pole
33. Temporal pole	**34.** Transverse temporal cortex
35. Insula cortex	

Fig. 4: *Cortical regions of interest index.* Each cortical hemisphere is parcellated using Desikan-Killiany cortical atlas. We display the cortical regions' names and their respective labels on the surface.